Magnetism, Spin Texture, and In-Gap States: Atomic Specialization at the Surface of Oxygen-Deficient SrTiO$_3$

Michaela Altmeyer,[1,*] Harald O. Jeschke,[1] Oliver Hijano-Cubelos,[2] Cyril Martins,[2] Frank Lechermann,[3,4]
Klaus Koepernik,[5] Andrés F. Santander-Syro,[6] Marcelo J. Rozenberg,[2] Roser Valentí,[1] and Marc Gabay[2]

[1]*Institut für Theoretische Physik, Goethe-Universität Frankfurt, 60438 Frankfurt am Main, Germany*
[2]*Laboratoire de Physique des Solides, Bat 510, Université Paris-Sud, 91405 Orsay, France*
[3]*I. Institut für Theoretische Physik, Universität Hamburg, 20355 Hamburg, Germany*
[4]*Institut für Keramische Hochleistungswerkstoffe, TU Hamburg-Harburg, D-21073 Hamburg, Germany*
[5]*IFW Dresden, Helmholtzstraße 20, 01069 Dresden, Germany*
[6]*CSNSM, Univ. Paris-Sud, CNRS/IN2P3, Université Paris-Saclay, Bât 104 et 108, 91405 Orsay, France*
(Received 1 December 2015; published 14 April 2016)

Motivated by recent spin- and angular-resolved photoemission (SARPES) measurements of the two-dimensional electronic states confined near the (001) surface of oxygen-deficient SrTiO$_3$, we explore their spin structure by means of *ab initio* density functional theory (DFT) calculations of slabs. Relativistic nonmagnetic DFT calculations display Rashba-like spin winding with a splitting of a few meV and when surface magnetism on the Ti ions is included, bands become spin-split with an energy difference ~100 meV at the Γ point, consistent with SARPES findings. While magnetism tends to suppress the effects of the relativistic Rashba interaction, signatures of it are still clearly visible in terms of complex spin textures. Furthermore, we observe an atomic specialization phenomenon, namely, two types of electronic contributions: one is from Ti atoms neighboring the oxygen vacancies that acquire rather large magnetic moments and mostly create in-gap states; another comes from the partly polarized t_{2g} itinerant electrons of Ti atoms lying further away from the oxygen vacancy, which form the two-dimensional electron system and are responsible for the Rashba spin winding and the spin splitting at the Fermi surface.

Introduction.—Transition metal oxides constitute a major topic of interest in the scientific community as these materials are endowed with a broad range of significant functionalities, ranging from ferroelectricity to metal-insulator transitions as well as from magnetism to superconductivity. Many of these compounds exhibit structural instabilities, strong electronic correlations, and complex phase diagrams with competing ground states. Artificial structures of transition metal oxides therefore seem ideal to explore interfacial effects that could possibly lead to new phases. In this respect, the observation a decade ago [1,2] of a two-dimensional electronic system (2DES) at the interface between the wide band-gap insulators LaAlO$_3$ (LAO) and SrTiO$_3$ (STO) has attracted a considerable amount of attention. It was found that the 2DES hosts gate-tunable insulator to metal, insulator to superconductor transitions, magnetism [3], and a large interfacial spin-orbit effect [4]. The mechanisms responsible for these special properties are still under debate. Questions include the intrinsic (i.e., electronic reconstruction) versus extrinsic (e.g., oxygen vacancies) mechanism [5–7] responsible for the formation of the 2DES, and also the role and spatial distribution of the various d orbitals that could contribute selectively to a specific charge or spin property.

Angular-resolved photoemission (ARPES) measurements revealed the existence of a 2DES with similar features to those seen at the LAO-STO interface at the bare surfaces of several insulating perovskite oxide crystals, and among them (001) oriented STO [8,9]. In this case, the carriers originate from oxygen vacancies. These vacancies are likely created during the sample preparation process and also when the sample is illuminated during the measurement [10]. Spin resolved ARPES (SARPES) measurements of the 2DES at the (001) oriented STO surface [11] have highlighted the existence of sizable Rashba-like spin textures along with a large energy splitting that has been interpreted as a signature of ferromagnetism. Their simultaneous occurrence is puzzling since the two effects *a priori* compete with each other and estimates of the respective energy scales give about 100 meV for magnetism and a few meV for surface spin-orbit coupling.

A number of density functional theory (DFT) studies on oxygen-deficient bulk STO [12–14] found magnetism and in-gap bound states below the conduction band. The reported location of the bound states and the size of the spin polarization depend strongly on the computational details. Recent nonmagnetic DFT calculations for slab geometries [15,16] found the formation of a 2DES at the surface, in addition to in-gap states. Effects of spin orbit coupling [17,18] and correlation [19] have also been studied at the model level.

In the present work, we investigate via first principles DFT the spin textures and magnetism of the 2DES states at

the (001) oriented surface of oxygen-deficient STO. As the preexisting literature on this problem is already large, let us emphasize that the new results reported here are relevant for the interpretation of the following experimental facts: (i) spin ARPES appears to highlight the occurrence of both Rashba-like textures and ferromagnetism [11], and (ii) ARPES spectra pertaining to the 2DES at interfaces and also at surfaces all seem to appear concomitant with a universal nondispersive feature at an energy of about 1.3 eV below the Fermi energy [20–22]. Our DFT calculations are accompanied by tight-binding model considerations.

Methods.—In order to extract the basic trends in the electronic properties we considered three representative slabs of (001) oriented STO with different oxygen vacancy concentrations and slab terminations in our DFT calculations: a single vacancy at the topmost level of a SrO-terminated $2 \times 2 \times 4$ slab [Fig. 1(a)], a vertical divacancy at the topmost level of a SrO-terminated $2 \times 2 \times 4$ slab [Fig. 1(a)], and a horizontal divacancy located at the topmost level of a TiO$_2$-terminated $3 \times 3 \times 4$ slab [Fig. 1(b), Ref. [23]]. These slabs are chosen as test cases for investigating the effects of surface reconstruction, in-gap states, Rashba spin-orbit coupling, and magnetism. We have made sure with a larger set of slabs (not shown) that all observations discussed below do not crucially depend on TiO$_2$ versus SrO termination. In all slabs we included a vacuum layer of at least 20 Å to avoid any spurious interactions between the periodic images. To our knowledge, no measurements of vacancy densities have been performed so far; therefore, we have chosen our test slabs such that the surface vacancy induced carrier densities are comparable to the experimental observations of $n_{2D} \approx$ 0.25–0.33 e^-/a^2 (see for instance Refs. [8,9,24]). Every vacancy nominally releases two electrons. Because of the in-gap state not all the additional electrons are contributing to the 2DES, so that we can estimate a required density of about one vacancy per 4 unit cells. Our mono- and

divacancy $2 \times 2 \times 4$ and $3 \times 3 \times 4$ slabs are therefore compatible with the experimental estimates.

In order to account for possible surface reconstructions, the internal coordinates of the slabs were relaxed with the projector-augmented wave basis [29] as implemented in VASP [30,31]. We used the generalized-gradient approximation (GGA) [32] in the Dudarev [33] GGA + U scheme as described in Ref. [15]. The electronic structure was analyzed with the all-electron full-potential local orbital (FPLO) [34] method and GGA + U functional [35]. Checks were also performed with the linearized augmented plane wave method as implemented in WIEN2K [36]. Spin textures for the various slabs were obtained from full relativistic calculations using the full-potential local orbital GGA + SO + U method with a newly implemented subroutine.

Results and discussion.—We start with the analysis of spin textures in the absence of magnetism. In Figs. 2(a) and 2(d) we show the spin textures (projections of the spin polarization vectors onto the xy plane) at the Fermi surface ($k_z = 0$) obtained for nonmagnetic ground states in GGA + SO + U calculations for the monovacancy $2 \times 2 \times 4$ and the divacancy $3 \times 3 \times 4$ slabs, respectively (results for the divacancy $2 \times 2 \times 4$ slab are shown in the Supplemental Material [25]). We used typical values for the parameters ($U = 5$ eV and $J_H = 0.64$ eV on Ti $3d$ orbitals [37]). In all cases, every two bands show a small energy splitting of a few meV due to the spin-orbit interaction. Spins at the Fermi surface ($k_z = 0$) are fully polarized in the xy plane, oppositely oriented in the split bands. On some of the bands the spins are pointing clock- and anticlockwise around Γ, which is a clear signature of the relativistic Rashba effect. On other bands we additionally notice a texture of rotating spins, born out of the more complex interplay between spin and orbital degrees of freedom [10,38]. The rather small size of the spin splitting contrasts with the large value reported in recent SARPES experiments [11].

Next, we consider solutions with ferromagnetic order and spin-orbit interactions. The ferromagnetic solution is indeed the ground state of the systems we consider [39]. Figure 2(b) displays the spin-projected band structure obtained from spin-polarized GGA + SO + U calculations for the monovacancy $2 \times 2 \times 4$ slab (similarly, results for the divacancy $2 \times 2 \times 4$ slab are shown in the Supplemental Material [25]). We adopt the magnetic moment quantization axis along z but below we also discuss the case of a quantization along x. The size of the magnetic splitting can be inferred from the black arrows connecting the majority and minority spin bands. For a comparison to the experiment we have to consider the splitting of the light bands of d_{xy} character, as heavy bands have been silenced in the measurements [11]. The energy separation at the Γ point of the two spin-split d_{xy} bands originating from Ti$_d$ [Fig. 1(a)] is of the order of 60 meV and in qualitative agreement with the experimental data [11] ($\Delta E \approx 100$ meV).

In order to identify the microscopic origin of the peculiar electronic and magnetic features described above we plot in
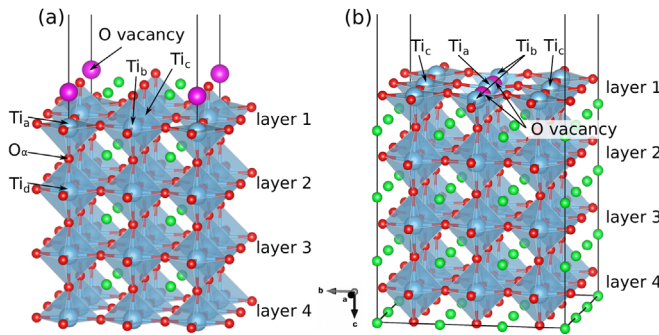

FIG. 1. (a) SrO-terminated $2 \times 2 \times 4$ slab with one oxygen vacancy at the topmost level. O$_\alpha$ denotes the position where a second vacancy is introduced for divacancy $2 \times 2 \times 4$ calculations (see text). (b) TiO$_2$-terminated $3 \times 3 \times 4$ slab with two vertically positioned oxygen vacancies. Other slab geometries are included in the Supplemental Material [25].
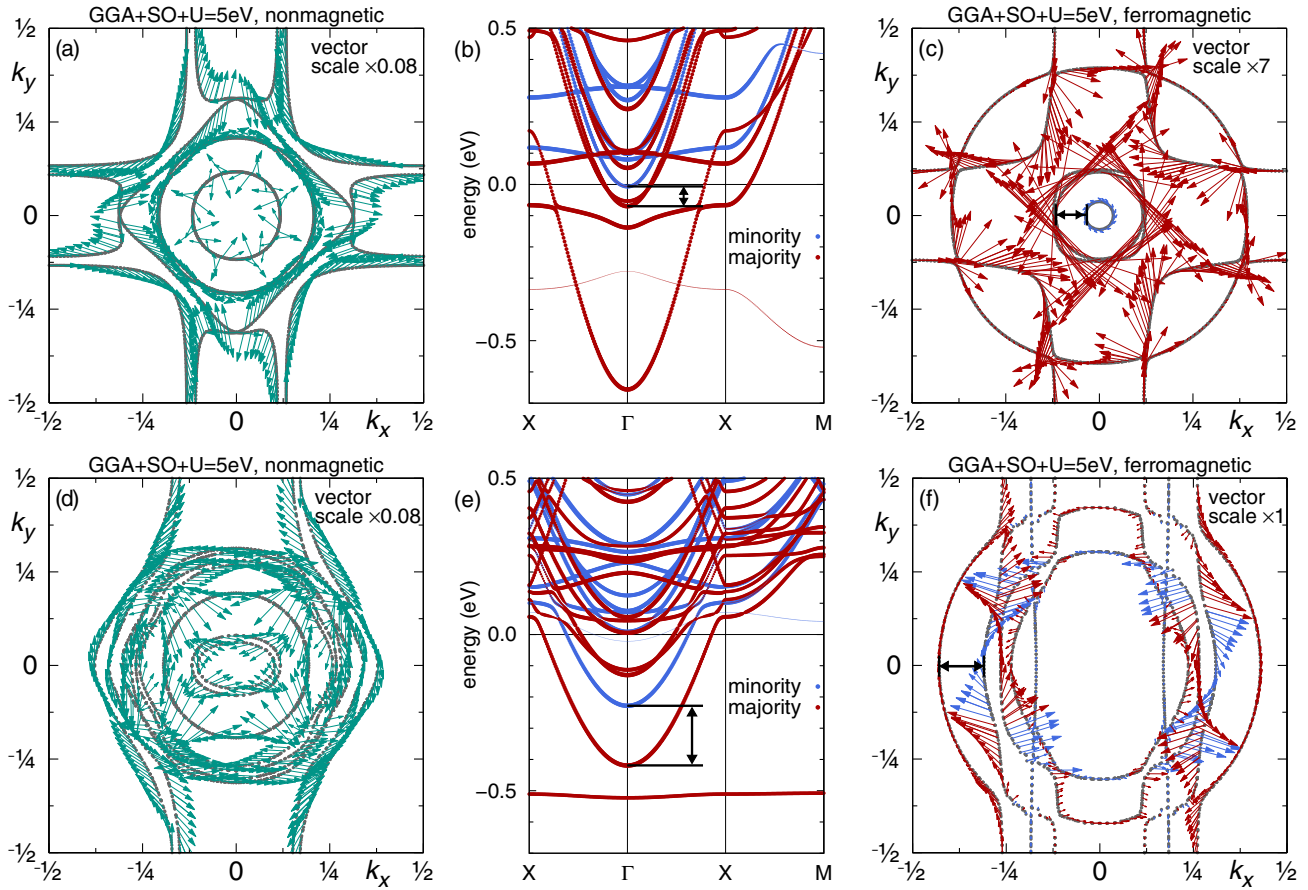
FIG. 2.   Spin textures and spin-polarized band structures for the monovacancy $2 \times 2 \times 4$ slab (a)–(c) and the divacancy $3 \times 3 \times 4$ slab (d)–(f). (a) and (d) are nonmagnetic GGA + SO + U calculations with $U = 5$ eV, and (b), (c), (e), and (f) are ferromagnetic GGA + SO + U calculations with $m \| \hat{z}$. Note that the large magnetic moments along $\hat{z}$ can be inferred from the exchange splitting in (b) and (e); the shown spin textures are projections on the xy plane. Reciprocal space units are $2\pi/(2a) = 0.805$ Å^{-1} for (a) and (c), and $2\pi/(3a) = 0.536$ Å^{-1} for (d) and (f), where a is the bulk STO lattice parameter. The different vector scales are chosen to enhance the visibility of the spin windings.

Fig. 3 the layer- and orbital-resolved GGA + SO + U band structure near E_F for the monovacancy $2 \times 2 \times 4$ slab and in Fig. 4(a) we display the Ti $t_{2g} - e_g$ resolved magnetic moments as a function of the distance between Ti and the O vacancy. We find that (i) the magnetic splitting of the light d_{xy} bands at the Fermi level is caused by itinerant electrons belonging to Ti located not in the immediate vicinity of the oxygen vacancy [e.g., Ti$_d$ in Fig. 1(a)] with Ti $3d$ magnetic moments of the order of $0.1\mu_B$ [see Fig. 4(a)], and (ii) Ti atoms neighboring the oxygen vacancy in the uppermost layer [Ti$_a$, Ti$_b$, Ti$_c$ in Fig. 1(a)] have the largest magnetic moment [Fig. 4(a)] and are mostly responsible for the heavy bands (Ti$_a$) and occupied states at higher binding energies (Ti$_b$, Ti$_c$, see Fig. 3). In particular, we observe an in-gap band of Ti e_g (d_{z^2}) character hybridizing with the Ti $4s$ and $4p$ orbitals corresponding to Ti$_a$. It sits at -0.4 eV in the single vacancy case and is shifted to about -1 eV in the $2 \times 2 \times 4$ divacancy case (see the Supplemental Material [25]). The position of this band depends on the parameters U and J_H chosen for the GGA + U calculations

and on the concentration and position of vacancies in the slab (see the Supplemental Material [25] and Ref. [16]).

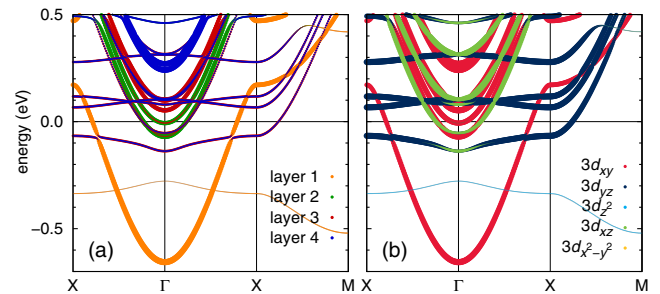Interestingly, already with this minimal slab, we find a phenomenon of atomic specialization; i.e., there are two

FIG. 3.   Ferromagnetic GGA + SO + U Ti $3d$ band structure for the monovacancy $2 \times 2 \times 4$ slab with $m \| \hat{z}$. (a) Layer resolved. (b) Orbitally resolved. Note that the thickness of the lines is proportional to the strength of the $3d$ character on the bands (the heavy band at -0.4 eV is strongly hybridized with the Ti $4s$ and $4p$ orbitals, see also the main text).

types of electronic contributions to magnetism: one from Ti atoms neighboring the oxygen vacancy that acquire rather large magnetic moments and are mostly located below the Fermi surface inducing in-gap states, and another, from those Ti atoms lying further away from the oxygen vacancies, that correspond to polarized t_{2g} itinerant electrons with small magnetic moments, which are responsible for the Rashba spin winding and the spin splitting at the Fermi surface. These remarkable effects will be even more pronounced in larger slabs.

We observe here the same phenomenon of atomic specialization as in the smaller $2 \times 2 \times 4$ slab: Ti atoms neighboring the oxygen vacancies [Ti_a and Ti_b in Fig. 1(b)] acquire large magnetic moments [see Fig. 4(b)] and are responsible for the in-gap states located at higher binding energies, while Ti atoms lying further away from the oxygen vacancy (Ti_c and beyond) contribute to the 2DES with itinerant electrons carrying small magnetic moments, which are responsible for the Rashba spin winding and the spin splitting at E_F [40].

Further insight into the atomic dichotomy can be gained through the tight-binding cluster diagonalization (see the Supplemental Material [25]) of structures with various configurations of vacancies. In order to monitor the formation of the 2DES conduction band states and of the in-gap states, we adiabatically turn on the energy contributions that represent the effect of introducing a vacancy into the cluster. Features seen in DFT are qualitatively reproduced.

Based on our above discussion of each individual effect, we may infer that spin textures and spin splitting compete with each other in the t_{2g} bands. Figure 2(c) displays the spin texture at $k_z = 0$ obtained from spin-polarized GGA + SO + U calculations for the monovacancy $2 \times 2 \times 4$ slab. The spin texture shows signs of the Rashba winding but it is less pronounced than in the

nonmagnetic case. Taking a closer look at the inner pockets in Fig. 2(c) (blue and red circles centered at Γ) corresponding to the spin up and spin down projections [compare Fig. 2(b)], we observe a significant Fermi momentum shift of the bands (~ 0.1 Å^{-1}), which is of the same order of magnitude as the one observed in SARPES experiments [11]. As can be inferred from the now very small in-plane spin component ($P_\parallel \leq 0.04$), ferromagnetism is dominating the arrangement of the spins but the spin winding is still visible. The same features are observed for the divacancy $3 \times 3 \times 4$ slab [Fig. 2(f)], confirming the general validity of the results. We have also checked the robustness of the results with respect to the choice of U in the GGA + U functional and find that the variation of U introduces only quantitative changes in the ferromagnetic calculations (see the Supplemental Material [25]).

Scanning superconducting quantum interference device measurements [3] on LAO/STO interfaces observed a preference of in-plane magnetic moments, which are ascribed to shape anisotropy. As this is also expected for pure STO surfaces, we additionally performed calculations with the magnetization axis along x; in this case the spins are aligned in plane and the Rashba interaction is unable to rotate the spins to achieve a sign change for opposite k points. However, a canting of the spin polarization vectors away from the magnetic axis originating from the Rashba coupling can be still identified, in agreement with previous theoretical considerations [41]. Our results would be compatible with SARPES spectra, which see both an almost pure Rashba spin texture and a full in-plane polarization, if we assume that the measurements detect a signal from a large number of ferromagnetic domains at once. In this case the effect of magnetism on the alignment of the spin polarization vectors is averaged out and the measured spin texture is completely determined by spin-orbit coupling effects, restoring the sign change for opposite k points and implying that the main features are independent of the magnetic quantization axis.

Conclusions.—By performing full relativistic nonmagnetic and magnetic density functional theory calculations in the framework of the GGA + SO + U functional on representative oxygen deficient SrTiO$_3$ slabs, we find the magnetic state to be the ground state and we observe clear signatures of atomic specialization of the electronic and magnetic contributions. Ti atoms neighboring the oxygen vacancies create e_g localized wave functions with large magnetic moments and are responsible for the presence of in-gap states at energies around -0.5 to -1 eV. The position of the in-gap states is influenced by the slab termination and the depth of the oxygen vacancy below the surface, and by possible oxygen clustering. On the other hand, Ti atoms lying further away from the oxygen vacancy contribute with polarized t_{2g} itinerant electrons to the conducting 2DES and are responsible for the Rashba spin winding and the spin splitting at the Fermi surface observed
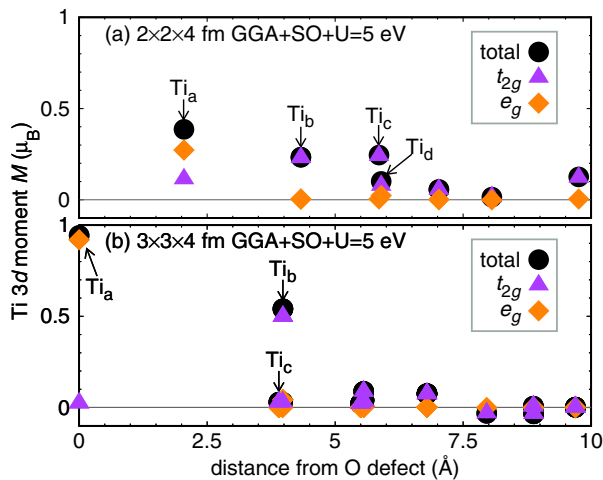

FIG. 4. t_{2g}-e_g resolved magnetic moments in GGA+SO+U= 5 eV for the (a) monovacancy $2 \times 2 \times 4$ and (b) divacancy $3 \times 3 \times 4$ slab in the ferromagnetic $m \| \hat{z}$ setup. Note that the moments shown do not contain hybridization contributions.

in SARPES. Our calculations show that magnetism masks the Rashba effect by increasing the spin splitting of the t_{2g} orbitals and by modifying the individual spin orientation but it does not eliminate spin winding. Considering that an averaging of inhomogeneities near the surface of the measured sample is to be expected (e.g., a sea of the 2DES interspersed with islands of magnetism perhaps mirroring a mixture of TiO_2 and SrO in the termination layer), SARPES measurements are explained by our calculations as the combined effect of the Rashba effect and magnetism.

---

*altmeyer@itp.uni-frankfurt.de

[1] A. Ohtomo and H. Y. Hwang, A high-mobility electron gas at the LaAlO₃/SrTiO₃ heterointerface, Nature (London) **427**, 423 (2004).

[2] S. Thiel, G. Hammerl, A. Schmehl, C. W. Schneider, and J. Mannhart, Tunable quasi-two-dimensional electron gases in oxide heterostructures, Science **313**, 1942 (2006).

[3] J. A. Bert, B. Kalisky, C. Bell, M. Kim, Y. Hikita, H. Y. Hwang, and K. A. Moler, Direct imaging of the coexistence of ferromagnetism and superconductivity at the LaAlO₃/SrTiO₃ interface, Nat. Phys. **7**, 767 (2011).

[4] J. A. Sulpizio, S. Ilani, P. Irvin, and J. Levy, Nanoscale phenomena in oxide heterostructures, Annu. Rev. Mater. Res. **44**, 117 (2014).

[5] V. Vonk, J. Huijben, D. Kukuruznyak, A. Stierle, H. Hilgenkamp, A. Brinkman, and S. Harkema, Polar-discontinuity-retaining A-site intermixing and vacancies at SrTiO₃/LaAlO₃ interfaces, Phys. Rev. B **85**, 045401 (2012).

[6] C. Cancellieri, D. Fontaine, S. Gariglio, N. Reyren, A. D. Caviglia, A. Fête, S. J. Leake, S. A. Pauli, P. R. Willmott, M. Stengel, Ph. Ghosez, and J.-M. Triscone, Electrostriction at the LaAlO₃/SrTiO₃ Interface, Phys. Rev. Lett. **107**, 056102 (2011).

[7] G. Berner, A. Müller, F. Pfaff, J. Walde, C. Richter, J. Mannhart, S. Thiess, A. Gloskovskii, W. Drube, M. Sing, and R. Claessen, Band alignment in LaAlO₃/SrTiO₃ oxide heterostructures inferred from hard x-ray photoelectron spectroscopy, Phys. Rev. B **88**, 115111 (2013).

[8] A. F. Santander-Syro, O. Copie, T. Kondo, F. Fortuna, S. Pailhes, R. Weht, X. G. Qiu, F. Bertran, A. Nicolaou, A. Taleb-Ibrahimi, P. Le Fevre, G. Herranz, M. Bibes, N. Reyren, Y. Apertet, P. Lecoeur, A. Barthelemy, and M. J. Rozenberg, Two-dimensional electron gas with universal subbands at the surface of SrTiO₃, Nature (London) **469**, 189 (2011).

[9] W. Meevasana, P. D. C. King, R. H. He, S-K. Mo, M. Hashimoto, A. Tamai, P. Songsiriritthigul, F. Baumberger, and Z-X. Shen, Creation and control of a two-dimensional electron liquid at the bare SrTiO₃ surface, Nat. Mater. **10**, 114 (2011).

[10] S. McKeown Walker, A. de la Torre, F. Y. Bruno, A. Tamai, T. K. Kim, M. Hoesch, M. Shi, M. S. Bahramy, P. D. C. King, and F. Baumberger, Control of a Two-Dimensional Electron Gas on SrTiO₃ (111) by Atomic Oxygen, Phys. Rev. Lett. **113**, 177601 (2014).

[11] A. F. Santander-Syro, F. Fortuna, C. Bareille, T. C. Roedel, G. Landolt, N. C. Plumb, J. H. Dil, and M. Radovic, Giant spin splitting of the two-dimensional electron gas at the surface of SrTiO₃, Nat. Mater. **13**, 1085 (2014).

[12] D. D. Cuong, B. Lee, K. M. Choi, H.-S. Ahn, S. Han, and J. Lee, Oxygen Vacancy Clustering and Electron Localization in Oxygen-Deficient SrTiO₃: LDA + U Study, Phys. Rev. Lett. **98**, 115503 (2007).

[13] Z. Hou and K. Terakura, Defect states induced by oxygen vacancies in cubic SrTiO₃: First-principles calculations, J. Phys. Soc. Jpn. **79**, 114704 (2010).

[14] A. Lopez-Bezanilla, P. Ganesh, and P. B. Littlewood, Magnetism and metal-insulator transition in oxygen-deficient SrTiO₃, Phys. Rev. B **92**, 115112 (2015).

[15] J. Shen, H. Lee, R. Valenti, and H. O. Jeschke, *Ab initio* study of the two-dimensional metallic state at the surface of SrTiO₃: Importance of oxygen vacancies, Phys. Rev. B **86**, 195119 (2012).

[16] H. O. Jeschke, J. Shen, and R. Valenti, Localized versus itinerant states created by multiple oxygen vacancies in SrTiO₃, New J. Phys. **17**, 023034 (2015).

[17] Z. Zhong, A. Tóth, and K. Held, Theory of spin-orbit coupling at LaAlO₃/SrTiO₃ interfaces and SrTiO₃ surfaces, Phys. Rev. B **87**, 161102 (2013).

[18] G. Khalsa, B. Lee, and A. H. MacDonald, Theory of t_{2g} electron-gas rashba interactions, Phys. Rev. B **88**, 041302 (2013).

[19] C. Lin and A. A. Demkov, Electron Correlation in Oxygen Vacancy in SrTiO₃, Phys. Rev. Lett. **111**, 217601 (2013).

[20] Y. Aiura, I. Hase, H. Bando, T. Yasue, T. Saitoh, and D. S. Dessau, Photoemission study of the metallic state of lightly electron-doped SrTiO₃, Surf. Sci. **515**, 61 (2002).

[21] R. Courths, Ultraviolet photoelectron spectroscopy (UPS) and LEED studies of BaTiO₃ (001) and SrTiO₃ (100) surfaces, Phys. Status Solidi B **100**, 135 (1980).

[22] Y. S. Kim, J. Kim, S. J. Moon, W. S. Choi, Y. J. Chang, J.-G. Yoon, J. Yu, J.-S. Chung, and T. W. Noh, Localized electronic states induced by defects and possible origin of ferroelectricity in strontium titanate thin films, Appl. Phys. Lett. **94**, 202906 (2009).

[23] In the $3 \times 3 \times 4$ slab [Fig. 1(b)] the loss of symmetry due to the presence of the vacancies induces a ladder of bands at E_F corresponding to inequivalent Ti atoms [Fig. 2(f)] and a breaking of the xy symmetry as also observed in the Fermi surface topography [Fig. 2(d)]. In experiment, such an

asymmetry is not observed and is here a consequence of considering an individual divacancy realization. This asymmetry is expected to decrease when larger slab geometries and a disorder average are considered, which is beyond our computational possibilities.

[24] The properties of the 2DES have been found to be independent of the bulk vacancy concentration [8].

[25] See Supplemental Material at http://link.aps.org/supplemental/10.1103/PhysRevLett.116.157203 for the discussion of other slab geometries, the analysis of the dependence on interaction strength U and tight binding calculations, which includes Refs. [26–28].

[26] H. Chen and A. J. Millis, Spin-density functional theories and their +U and +J extensions: A comparative study of transition metals and transition metal oxides, Phys. Rev. B **93**, 045133 (2016).

[27] L. F. Mattheiss, Energy bands for $KNiF_3$, $SrTiO_3$, $KMoO_3$ and $KTaO_3$, Phys. Rev. B **6**, 4718 (1972).

[28] J. Slater and G. Koster, Simplified LCAO method for the periodic potential problem, Phys. Rev. **94**, 1498 (1954).

[29] P. E. Blöchl, Projector augmented-wave method, Phys. Rev. B **50**, 17953 (1994).

[30] G. Kresse and J. Furthmüller, Efficiency of *ab initio* total energy calculations for metals and semiconductors using a plane-wave basis set, Comput. Mater. Sci. **6**, 15 (1996).

[31] J. Hafner, Ab-initio simulations of materials using vasp: Density-functional theory and beyond, J. Comput. Chem. **29**, 2044 (2008).

[32] J. P. Perdew, K. Burke, and M. Ernzerhof, Generalized Gradient Approximation made Simple, Phys. Rev. Lett. **77**, 3865 (1996).

[33] S. L. Dudarev, G. A. Botton, S. Y. Savrasov, C. J. Humphreys, and A. P. Sutton, Electron-energy-loss spectra and the structural stability of nickel oxide: An LSDA + U study, Phys. Rev. B **57**, 1505 (1998).

[34] K. Koepernik and H. Eschrig, Full-potential nonorthogonal local-orbital minimum-basis band-structure scheme, Phys. Rev. B **59**, 1743 (1999).

[35] A. I. Liechtenstein, V. I. Anisimov, and J. Zaanen, Density-functional theory and strong interactions: Orbital ordering in Mott-Hubbard insulators, Phys. Rev. B **52**, R5467 (1995).

[36] P. Blaha, K. Schwarz, G. K. H. Madsen, D. Kvasnicka, and J. Luitz, WIEN2K, An Augmented Plane Wave and Local Orbitals Program for Calculating Crystal Properties, Techn. Universität Wien, Austria, 2001.

[37] S. Okamoto, A. J. Millis, and N. A. Spaldin, Lattice Relaxation in Oxide Heterostructures: $LaAlO_3/SrTiO_3$ Superlattices, Phys. Rev. Lett. **97**, 056802 (2006).

[38] P. D. C. King, S. McKeown Walker, A. Tamai, A. de la Torre, T. Eknapakul, P. Buaphet, S.-K. Mo, W. Meevasana, M. S. Bahramy, and F. Baumberger, Quasiparticle dynamics and spin-orbital texture of the $SrTiO_3$ two-dimensional electron gas, Nat. Commun. **5**, 3414 (2014).

[39] At the $GGA + SO + U = 5$ eV level, the ferromagnetic solution lowers the energy by 14.9 meV per formula unit (f.u.) for a single O vacancy in the $2 \times 2 \times 4$ slab, and by 7.3 meV/f.u. for a divacancy in the $3 \times 3 \times 4$ slab; the difference in stabilization energy arises from the respective total moments of $0.125\mu_B$/f.u. and $0.077\mu_B$/f.u., which are averaged over the 16 and 36 formula units of the two slabs.

[40] We note that due to the special divacancy geometry, the neighboring Ti_b create dominantly d_{xz} in-gap states at -0.5 eV while the heavy e_g band of Ti_a in Fig. 1(b) appears at the Fermi surface. A different arrangement of the divacancy in this slab has been found [16] to shift the heavy e_g state to the gap region consistent with experimental observations.

[41] S. E. Barnes, J. Ieda, and S. Maekawa, Rashba spin-orbit anisotropy and the electric field control of magnetism, Sci. Rep. **4**, 4105 (2014).